

# Closed-Loop Sensitivity Identification for Cross-Directional Systems

Callum Umana Stuart<sup>†</sup> and Idris Kempf<sup>\*</sup>

**Abstract**—At Diamond Light Source, the UK’s national synchrotron facility, electron beam disturbances are attenuated by the fast orbit feedback (FOFB), which controls a cross-directional (CD) system with hundreds of inputs and outputs. Due to the inability to measure the disturbance spectrum in real-time, the closed-loop sensitivity of the FOFB cannot be evaluated, making it difficult to compare FOFB algorithms and detect faults. Existing methods rely on comparing open-loop with closed-loop measurements, but they are prone to instabilities and actuator saturation because of the system’s strong directionality. Here, we introduce a reference signal to estimate the complementary sensitivity in closed loop. By decoupling the system into sets of single-input, single-output (SISO) systems, we design the reference mode-by-mode to accommodate the system’s strong directionality. This allows SISO system identification to be used, making our approach suitable for large-scale systems. Additionally, we derive lower bounds on reference amplitudes to achieve a predefined estimation error bound in the presence of disturbances and measurement noise. Our approach not only enables performance estimation of ill-conditioned CD systems in closed-loop but also provides a signal for fault detection. Its potential applications extend to other CD systems, such as papermaking, steel rolling, or battery manufacturing processes.

## I. INTRODUCTION

Diamond Light Source (Diamond) is the UK’s national synchrotron facility that produces *synchrotron radiation* for research, such as investigating material properties, biological structures, or chemical reactions. The radiation is emitted by electrons circulating at relativistic speeds within the *storage ring*. A critical factor in synchrotron performance is the brightness of the synchrotron radiation, which can be significantly impacted by electron beam vibrations. The vibrations are attenuated by the fast orbit feedback (FOFB) system that uses hundreds of *corrector magnets* (inputs) and *beam position monitors* (outputs) at a rate  $\geq 10$  kHz. The dynamics of the electron beam are modelled by a cross-directional system [1]:

$$y(s) = Rg(s)u(s) + d(s), \quad (1)$$

where  $s \in \mathbb{C}$  is the Laplace variable,  $R \in \mathbb{C}^{n_y \times n_u}$  the *response matrix*,  $g : \mathbb{C} \rightarrow \mathbb{C}$  the scalar actuator dynamics,  $u : \mathbb{C} \rightarrow \mathbb{C}^{n_u}$  are the inputs,  $y : \mathbb{C} \rightarrow \mathbb{C}^{n_y}$  the outputs and  $d : \mathbb{C} \rightarrow \mathbb{C}^{n_y}$  the disturbances, such as vibrations of the girders or (electro)magnetic fields. The separation of

the plant  $P(s) := Rg(s)$  into a matrix of constant values and a scalar dynamic term allows (1) to be diagonalised using the singular value decomposition (SVD)  $R = U\Sigma V^T$ , which is referred as the *modal transformation* [2]. Most CD controllers combine a pseudo-inverse  $R^\dagger$  with a scalar controller  $q(s)$  that (partially) inverts the actuator dynamics. Other examples of (large-scale) CD systems can be found in process engineering, paper making, web processes, and metal rolling [3].

For synchrotron applications, the response matrix is ill-conditioned with condition numbers  $\kappa(R) := \|R\|_2/\|R^\dagger\|_2$  ranging from  $10^3$  to  $10^4$  [1], making (1) prone to actuator saturation and sensitive to modelling errors [4]. For synchrotron operation, it is crucial that the FOFB meets the theoretical performance specifications, i.e. that the *sensitivity*  $S : \mathbb{C}^{n_y} \rightarrow \mathbb{C}^{n_y}$  in  $y(s) = S(s)d(s)$  has the expected gains. However,  $d(s)$  cannot be measured when the FOFB is operational, prohibiting  $S(s)$  to be estimated in closed-loop.

To identify the estimate  $\hat{S}(s)$ , existing methods rely on comparing open-loop with closed-loop measurements. One approach is to compute [5]  $\|y^{\text{cl}}(j\omega)\|_2/\|y^{\text{ol}}(j\omega)\|_2$ , where

$$y^{\text{cl}}(s) = S(s)d(s) - T(s)n(s), \quad (2a)$$

$$y^{\text{ol}}(s) = d(s) + n(s), \quad (2b)$$

and  $n(s)$  is the measurement noise and  $T(s) := I - S(s)$  the *complementary sensitivity*. However, the disturbance spectrum  $d(s)$  can be time-varying and the 2-norm inappropriate for systems with large  $\kappa(R)$ . Another approach [6] is to add a signal  $r_u(s)$  to the plant input and measure the output in open and closed loop, so that  $y^{\text{ol}}(s) = P(s)r_u(s) + d(s)$  and  $y^{\text{cl}}(s) = S(s)P(s)r_u(s) + S(s)d(s)$ . If  $r_u(s) = e_i\rho_i(s)$  with  $e_i$  being the  $i$ th standard basis vector and  $\rho_i : \mathbb{C} \mapsto \mathbb{C}$  a scalar function, the ratio  $y_i^{\text{cl}}(s)/y_i^{\text{ol}}(s)$  for the  $i$ th output is

$$\frac{y_i^{\text{cl}}(s)}{y_i^{\text{ol}}(s)} = \frac{\sum_j S_{i,j}(s)P_{j,i}(s)\rho_i(s) + S_{i,i}(s)d_i(s)}{P_{i,i}(s)\rho_i(s) + d_i(s)}.$$

For  $\|P_{i,i}(s)\rho_i(s)\|_2 \gg \|d_i(s)\|_2$ ,

$$\frac{y_i^{\text{cl}}(s)}{y_i^{\text{ol}}(s)} \approx \frac{\sum_j S_{i,j}(s)P_{j,i}(s)}{P_{i,i}(s)},$$

from which  $S_{i,i}$  can be estimated if the system is diagonally dominant [7], i.e. if  $|P_{i,i}(j\omega)| \gg |P_{j,i}(j\omega)| \forall j \neq i$ . However, the requirement  $|P_{i,i}(j\omega)\rho_i(j\omega)| \gg |d_i(j\omega)|$  may destabilise the electron beam in open-loop and  $|P_{i,i}(j\omega)| \gg |P_{j,i}(j\omega)|$  cannot be satisfied for every  $i$  when  $\kappa(R)$  is large.

Both authors are with the Department of Engineering Science, University of Oxford, Oxford, UK.

<sup>†</sup>C. U. S. was supported by the Engineering Undergraduate Research Opportunities Programme (EUROP) scheme of the Department of Engineering Science, University of Oxford, Oxford, UK.

\*Corresponding author: idris.kempf@eng.ox.ac.uk

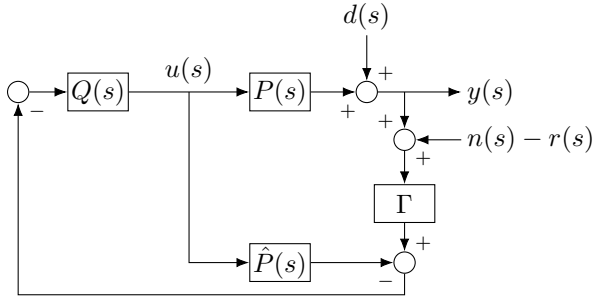


Fig. 1: IMC structure with plant  $P(s)$ , plant model  $\hat{P}(s)$ , IMC filter  $Q(s)$ , compensator  $\Gamma$ , disturbance  $d(s)$ , noise  $n(s)$ , and reference signal  $r(s)$ .

In this paper, we propose introducing an output reference signal  $r: \mathbb{C} \mapsto \mathbb{C}^{n_y}$ , so that the closed loop becomes

$$y(s) = S(s)d(s) + T(s)r(s) - T(s)n(s). \quad (3)$$

Below the closed-loop bandwidth, it holds that  $\|r(j\omega)\|_2 \gg \|S(j\omega)d(j\omega)\|_2$  and  $\|r(j\omega)\|_2 \gg \|n(j\omega)\|_2$ , allowing  $T(s)$  to be estimated from (3), even for small  $\|r(s)\|_2$ . However, due to the large condition number of  $R$ , setting  $r(s) = e_i \rho_i(s)$  may lead to large actuator gains or require to limit the amplitude of  $r(s)$ , impacting the accuracy of the estimates,  $\hat{T}(s)$  and  $\hat{S}(s)$ . To address this, the modal transformation is applied to (1) and the reference signal designed in modal space, tuning it to the gain and bandwidth of the modes. Based on the orthogonality of the modal transformation, lower bounds on  $\|r(j\omega)\|_2$  are defined to meet a predefined estimation accuracy, which are then juxtaposed with input amplitude and rate constraints. Finally, we provide simulation results using real-world disturbance data from Diamond to evaluate the efficacy of our method, currently being implemented at Diamond.

*Notation and Definitions* For a scalar, vector or matrix  $A$ , let  $A^T$  ( $A^*$ ) its (Hermitian) transpose,  $\text{diag}(A_1, \dots, A_n)$  a diagonal matrix with diagonal elements  $A_1, \dots, A_n$ . Let  $I_n$  denote the identity matrix in  $\mathbb{R}^{n \times n}$ . For a matrix  $A$ , let  $A^\dagger$  denote the pseudo-inverse [8, p. 290],  $\|A\|_2$  the spectral norm, and  $\kappa(A) := \|A\|_2 / \|A^\dagger\|_2$  the condition number.

## II. MODAL REPRESENTATION

### A. System

Although our method is applicable to any controller structure, this paper focuses on the *internal model control* (IMC) structure used at Diamond [5], as shown in Fig. 1. To design the reference  $r(s)$ , the MIMO representation (1) is mapped to modal space by substituting the thin SVD,  $R = U\Sigma V^T$  [2]:

$$\tilde{y}(s) = \Sigma g(s)\tilde{u}(s) + \tilde{d}(s), \quad (4)$$

where  $\tilde{y}(s) := U^T y(s)$ ,  $\tilde{d}(s) := U^T d(s)$ , and  $\tilde{u}(s) := V^T u(s)$ . The matrices  $U$  and  $V$  satisfy  $U^T U = I$  and  $V^T V = I$  and  $\Sigma := \text{diag}(\sigma_1, \dots, \sigma_{n_y})$  is a diagonal matrix containing the singular values. Throughout the paper it is assumed that  $\text{rank}(R) = n_y \leq n_u$ , which holds for Diamond, but our results remain valid for other configurations.

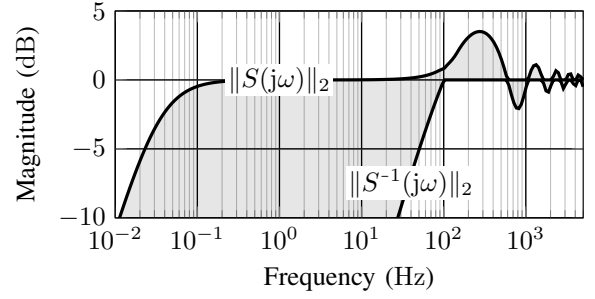


Fig. 2: Minimum and maximum sensitivity gains.

### B. Controller

In modal space, the IMC filter  $\tilde{Q}(s) := V^T Q(s)U$  is diagonal with elements  $q_i(s) := \lambda(s)/(\sigma_i g(s))$  [5], where  $\lambda(s)$  contains the non-minimum phase parts of  $g(s)$  and shapes the overall bandwidth. The compensator  $\tilde{\Gamma} := U^T \Gamma U$  attenuates controller gains for small  $\sigma_i$  and is diagonal with elements  $\gamma_i := \sigma_i^2 / (\sigma_i^2 + \mu)$ , where  $\mu > 0$  is a scalar regularisation parameter. For an accurate plant model ( $\hat{P}(s) \equiv P(s)$ ), this results in the modal inputs (see [9])

$$\tilde{u}_i(s) = -\frac{\gamma_i}{\sigma_i} \frac{\lambda(s)/g(s)}{1 - (1 - \gamma_i)\lambda(s)} (\tilde{d}_i(s) + \tilde{n}_i(s) - \tilde{r}_i(s)), \quad (5)$$

and the modal outputs

$$\tilde{y}_i(s) = \tilde{S}_i(s)\tilde{d}_i(s) + \tilde{T}_i(s)(\tilde{r}_i(s) - \tilde{n}_i(s)), \quad (6)$$

for  $i = 1, \dots, n_y$ , and where  $\tilde{S}_i(s) = 1 - \tilde{T}_i(s)$  and

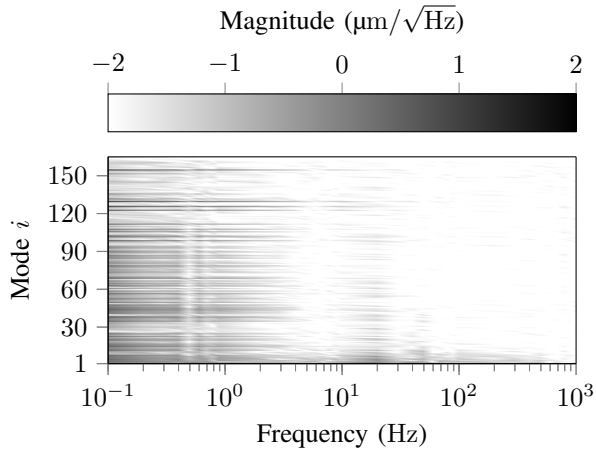
$$\tilde{T}_i(s) =: \gamma_i \frac{\lambda(s)}{1 - (1 - \gamma_i)\lambda(s)}. \quad (7)$$

The sensitivities in original space are obtained from  $T(s) := U \text{diag}(\tilde{T}_1(s), \dots, \tilde{T}_{n_y}(s))U^T$  and  $S(s) := U \text{diag}(\tilde{S}_1(s), \dots, \tilde{S}_{n_y}(s))U^T$ . The minimum and maximum gains of  $S(s)$  are shown in Fig. 2 for the Diamond system (see Section IV), where  $\|S(j\omega)\|_2 \equiv |\tilde{S}_{n_y}(j\omega)|$  and  $\|S^{-1}(j\omega)\|_2 \equiv |\tilde{S}_1(j\omega)|$  for frequencies below 100 Hz. Due to the large  $\kappa(R)$ , the compensator  $\Gamma$  effectively reduces the bandwidth for higher-order modes, leading to a significant difference between minimum and maximum gains of  $S(s)$ . The reduction in bandwidth for higher-order modes is justified by the characteristic spectrum of  $\tilde{d}(s)$ . Fig. 3a shows the amplitude spectral density of the output in mode space for disabled FOFB, i.e. when  $\tilde{y}^{\text{ol}}(s) = \tilde{d}(s) + \tilde{n}(s)$ . For low frequencies for which  $\|\tilde{d}(j\omega)\|_2 \gg \|\tilde{n}(j\omega)\|_2$ , the spectrum of  $\tilde{y}^{\text{ol}}(s)$  is proportional to the square of the singular values [10]. The simulated attenuation is shown in Fig. 3b, i.e. when  $\tilde{y}^{\text{cl}}(s) = \tilde{S}(s)\tilde{d}(s) - \tilde{T}(s)\tilde{n}(s)$ . The dashed line represents the bandwidth ( $-3$  dB frequency) of  $\tilde{S}_i(s)$ .

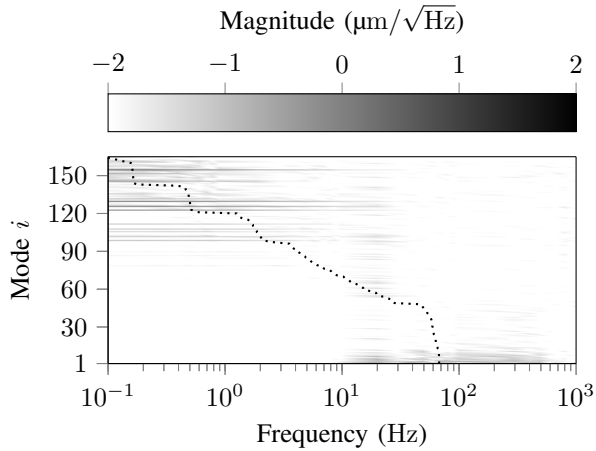
### C. Reference

While fixing the reference in original space as  $r(s) = e_i \rho_i(s)$  can cause large inputs, fixing the reference in modal space as

$$\tilde{r}(s) = e_i \rho_i(s) \quad \Rightarrow \quad r(s) = U_i \rho_i(s), \quad (8)$$



(a) Amplitude spectral density of  $\tilde{y}^{ol}(s)$ .



(b) Amplitude spectral density of  $\tilde{y}^{cl}(s)$  and bandwidth of  $\tilde{S}_i(j\omega)$  (dotted).

Fig. 3: Spectral density of output in mode space.

where  $U_i$  is the  $i$ th column of  $U$ , allows  $r(s)$  to be tuned mode-by-mode through adapting  $\rho_i(s)$ . Moreover, since the modal closed-loop dynamics (6) are decoupled, the (complementary) sensitivity can be estimated from  $\rho_i(s)$  and  $\tilde{y}_i(s)$  using SISO techniques.

With the reference (8) applied to mode  $i$ , it holds that  $\tilde{y}_i(s) = \Delta\tilde{y}_i(s) + \tilde{T}_i(s)\rho_i(s)$  and  $\tilde{y}_j(s) = \Delta\tilde{y}_j(s)$ ,  $j \neq i$ , where

$$\Delta\tilde{y}_i(s) := \tilde{S}_i(s)\tilde{d}_i(s) - \tilde{T}_i(s)\tilde{n}_i(s), \quad i = 1, \dots, n_y. \quad (9)$$

The terms (9) introduce an estimation error. For an estimate  $\hat{T}_i(j\omega) := \tilde{y}_i(j\omega)/\rho_i(j\omega)$ , the absolute estimation error is

$$\tilde{\epsilon}_i(j\omega) := |\hat{T}_i(j\omega) - \tilde{T}_i(j\omega)| = |\Delta\tilde{y}_i(j\omega)/\rho_i(j\omega)|. \quad (10)$$

To bound  $\tilde{\epsilon}_i(j\omega) \leq \epsilon_{\max}$  for frequencies of interest,  $\omega \leq \hat{\omega}_i$ , the reference signal must therefore satisfy the lower bound

$$|\rho_i(j\omega)| \geq \frac{1}{\epsilon_{\max}} \times |\tilde{S}_i(j\omega)\tilde{d}_i(j\omega) - \tilde{T}_i(j\omega)\tilde{n}_i(j\omega)|, \quad (11)$$

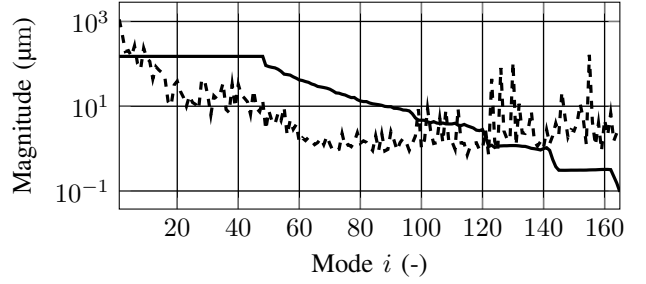


Fig. 4: Lower (dashed) and upper bounds on the reference amplitude for  $u_{\max} = 1$  A,  $y_{\max} = 150$   $\mu\text{m}$ , and  $\epsilon_{\max} = 0.1$ .

Since  $U^T U = I$ , the resulting estimation error in original space is then bounded by

$$\|T(j\omega) - \hat{T}(j\omega)\|_2 = \|\tilde{T}(j\omega) - \hat{\tilde{T}}(j\omega)\|_2 \leq \epsilon_{\max}. \quad (12)$$

Although a large  $|\rho_i(j\omega)|$  reduces the estimation error (10), system (1) is limited by component-wise input and output constraints,  $|u_i(t)| \leq u_{\max}$  and  $|y_i(t)| \leq y_{\max}$  [11]. Assuming that  $r(s)$  is a cosine at frequency  $\omega$  with  $|r(j\omega)| \gg \max(|d(j\omega)|, |n(j\omega)|)$ , the input and output constraints are approximated in frequency domain by

$$|u_i(j\omega)| \leq u_{\max}, \quad |y_i(j\omega)| \leq y_{\max}. \quad (13)$$

Since  $V^T V = I$ , it holds that  $|u_i(j\omega)| \leq \|u(j\omega)\|_2 = \|\tilde{u}(j\omega)\|_2$ , and assuming that  $|\tilde{r}_i(j\omega)| \gg |\tilde{d}_i(j\omega) - \tilde{n}_i(j\omega)|$  for  $\omega \leq \hat{\omega}_i$  in (5),  $\|\tilde{u}(j\omega)\|_2 \approx |\tilde{u}_i(j\omega)|$  for a reference as in (8). To limit  $|u_i(j\omega)| \leq u_{\max}$ , the reference must therefore satisfy

$$|\rho_i(j\omega)| \leq \frac{u_{\max}\sigma_i}{\gamma_i} \times \frac{1 - (1 - \gamma_i)\lambda(j\omega)}{\lambda(j\omega)/g(j\omega)}. \quad (14)$$

Similarly, to limit  $|y_i(j\omega)| \leq y_{\max}$ , the reference must satisfy

$$|\rho_i(j\omega)| \leq y_{\max}. \quad (15)$$

The lower and upper bounds for the case that  $\rho_i(j\omega)$  is a chirp signal (Section III) with amplitude  $A_i$  are shown in Fig. 4. The upper bound (solid) is computed from the minimum of (14) and (15), and the lower bound (dashed) from (11) for  $\epsilon_{\max} = 0.1$  and includes an additional factor introduced by windowing (Section III). Due to the large  $\kappa(R)$ , higher-order modes ( $i \geq 100$ ) require significantly larger control inputs than lower-order modes. However, the upper bound (14) limits  $A_i$ , which can result in estimation errors larger than  $\epsilon_{\max}$ . The large  $\kappa(R)$  also impacts lower-order modes through large disturbances (Fig. 3a), resulting in a low signal-to-noise ratio. Even though (14) would allow for larger  $A_i$ , lower-order modes are limited by (15).

### III. SENSITIVITY IDENTIFICATION

To identify the sensitivity, the reference signal is swept from  $\omega = 0$  to  $\omega = \hat{\omega}_i$  for each mode  $i = 1, \dots, n_y$ , i.e.

$$\rho_i(t) = A_i \cos\left(\frac{\hat{\omega}_i t}{NT_s} t\right), \quad t \in [0, NT_s],$$

where  $N$  is the number of samples and  $T_s$  the sample time. To avoid input and output saturation, the maximum frequency  $\hat{\omega}_i$  of the reference signal for each mode is set to 5 times the bandwidth of (7). The amplitude  $A_i$  is set to the upper bound from Fig. 4. After mapping the closed-loop data to mode space, the estimate  $\hat{T}_i(j\omega)$  is obtained from the Blackman-Tuckey spectral analysis method [12, Ch. 6]:

$$\hat{T}_i(j\omega) := \frac{\hat{\Phi}_{\tilde{y}_i \rho_i}(\omega)}{\hat{\Phi}_{\rho_i \rho_i}(\omega)} := \frac{\sum_{\tau=-M}^M \hat{R}_{\tilde{y}_i \rho_i}(\tau) W_M(\tau) e^{j\omega t}}{\sum_{\tau=-M}^M \hat{R}_{\rho_i \rho_i}(\tau) W_M(\tau) e^{j\omega t}}, \quad (16)$$

where  $W_M(\tau)$  is a Hamming window and the correlation functions are computed in modal space as

$$\hat{R}_{v_i w_i}(\tau) := \frac{1}{N} \sum_{t=1}^N v_i(t + \tau) w_i(t). \quad (17)$$

The windowing function allows for a smoothed spectral estimate of the complementary sensitivity by computing a weighted average of the frequency response of neighboring points. Large windows (small  $M$ ) filter out the variance from (10) but introduce bias, which is particularly visible for low frequencies at which  $\tilde{T}_i(s) \approx 1$ . The converse is true for small windows, and the trade-off between bias and variance must be considered when selecting an  $M$  value (note that  $M$  is denoted as  $\gamma$  in [12, Ch. 6]). Here, the parameter  $M$  is chosen to proportionally to  $1/\hat{\omega}_i$ , ranging from  $M = 500$  for mode  $i = 1$  to  $M = 14000$  for  $i = n_y$ . Note that a windowing factor is included in the lower bound of Fig. 4.

Although the complementary sensitivity is estimated in closed-loop, the reference  $r(s) = e_i \rho(s)$  is not correlated with the disturbance  $d(s)$  or the noise  $n(s)$ , avoiding closed-loop issues encountered in plant identification [13]. The identification procedure is summarised in Algorithm 1, where  $U_i$  refers to column  $i$  of the modal transformation matrix  $U$  (Section II). Neglecting the complexity of the data collection and the mapping of the signals to mode space, Algorithm 1 is of complexity  $n_y \times \mathcal{O}(\hat{T}_i)$ , where  $\mathcal{O}(\hat{T}_i)$  is the complexity of estimating the scalar transfer function  $\hat{T}_i$ . Without the modal representation, estimating  $T(s)$  would be of complexity  $n_y^2 \times \mathcal{O}(\hat{T}_i)$ .

---

**Algorithm 1** Sensitivity identification in modal space.

---

**Input:**  $u_{\max}, \epsilon_{\max}$

**Output:**  $S(j\omega)$

- 1: **for**  $i = 1$  to  $n_y$  **do**
  - 2:   Collect closed-loop data  $y^{\text{cl}}(t)$  for  $r(t) = U_i \rho_i(t)$
  - 3:   Map to modal space via  $\tilde{y}^{\text{cl}}(t) = U^T y^{\text{cl}}(t)$
  - 4:   Compute  $\hat{T}_i(j\omega)$  using  $\tilde{y}^{\text{cl}}(t)$  and  $\rho_i(t)$
  - 5: **end for**
  - 6: Set  $\hat{T}(j\omega) = U \hat{T}_i(j\omega) U^T$  and  $S(j\omega) = I - \hat{T}(j\omega)$
- 

## IV. SIMULATIONS

At Diamond, the FOFB uses  $n_y = 173$  sensors and  $n_u = 172$  magnets operated at  $f_s = 10$  kHz. However, the FOFB can be reconfigured, allowing any combination of  $n_y \leq 173$  sensors and  $n_u \leq 172$  outputs and inputs. For these simulations, it is assumed that  $n_y = n_u = 165$  with  $\kappa(R) = 9837$  ( $\sigma_{\max} = 195$  and  $\sigma_{\min} = 0.02$ ),  $u_{\max} = 5$  A, and  $y_{\max} = 150 \mu\text{m}$ . The actuator dynamics are  $g(s) = a/(s + a)e^{-\tau_d s}$  with  $a = 2\pi \times 700 \text{ rad s}^{-1}$  and a time delay  $\tau_d = 900 \mu\text{s}$  [9]. The transfer function  $\lambda(s)$  is  $\lambda(s) = \bar{\lambda}/(s + \bar{\lambda})e^{-\tau_d s}$  with  $\bar{\lambda} = 2\pi \times 176 \text{ rad s}^{-1}$  and the regularisation parameter is set to  $\mu = 1$ . As reflected in Fig. 2, the large time delay causes a sensitivity overshoot of 3.5 dB and the large  $\kappa(R)$  bandwidths of  $\tilde{S}_i(s)$  that spread from 0.03 Hz to 70 Hz (Fig. 3a).

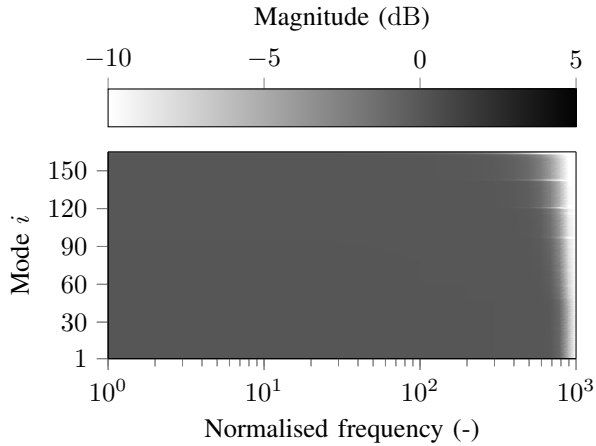
To evaluate the Algorithm 1 and verify the bound (11) with  $\epsilon_{\max} = 0.1$  for Diamond, the closed-loop system (3) was simulated using  $10^5$  measured disturbance samples from Diamond, which were different from the  $10^4$  samples used to compute the bounds in Fig. 4. The reference signal was chosen as in Section III and Algorithm 1 evaluated 10 times for  $N = 10^4$  samples. The estimates are computed using Matlab System Identification Toolbox on a desktop computer (Intel i7-7700 CPU @ 3.1 GHz, 8 GB) within less than 3 min for all 165 modes.

The magnitudes of the true complementary sensitivity in modal space,  $\tilde{T}(j\omega)$ , the average of the estimates,  $E\{\hat{T}(j\omega)\}$ , and the mean absolute error,  $E\{|\hat{T}(j\omega) - \tilde{T}(j\omega)|\}$  are shown in Fig 5a–5c. The horizontal axis refers to the normalised frequency that ranges from 0 to  $\hat{\omega}_i$  for each mode. Fig. 5c shows that for higher-order modes for which the lower bounds from Fig. 4 are violated, the resulting estimation error is larger than  $\epsilon_{\max}$ . However, for lower-order modes, the estimation error is below  $\epsilon_{\max}$  as expected from Fig. 4.

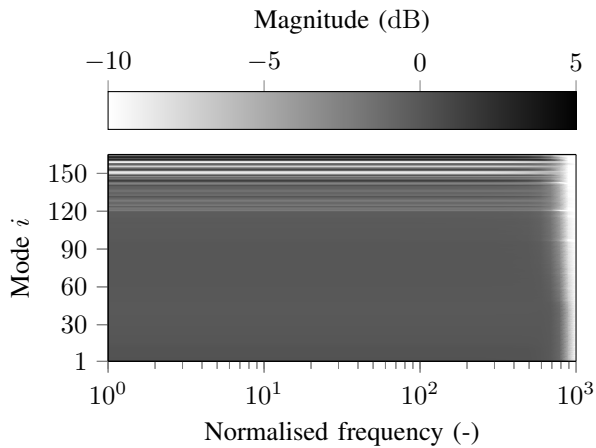
The maximum input amplitudes  $\max_j |\tilde{u}_j(t)|$  and  $\max_j |u_j(t)|$  for a reference signal on mode  $i$  are shown in Fig. 6. For all modes, it holds that  $\max_i |\tilde{u}_i(j\omega)| \leq 1.5$  A, which is below the limit  $u_{\max} = 5$  A. This is related to the frequency-domain approximation (13) and to choosing a constant (frequency-independent) amplitude of the chirp. As expected from the orthogonality from the modal transformation, it holds that  $\max_j |\tilde{u}_j(t)| \leq \max_j |u_j(t)|$ .

## V. CONCLUSION

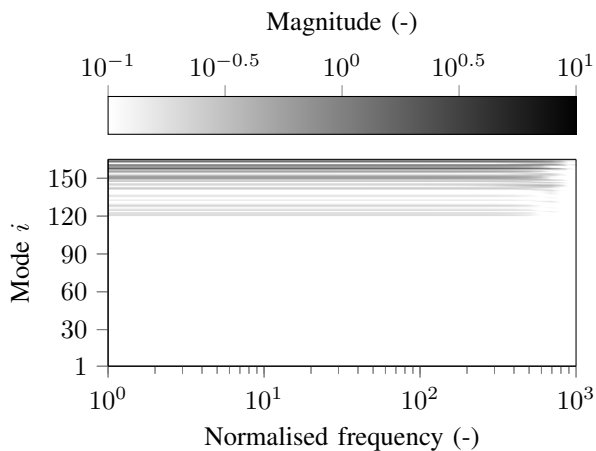
In this paper, we have proposed an algorithm for closed-loop sensitivity identification for ill-conditioned cross-directional systems and evaluated it using Diamond's electron beam stabilisation problem. While the controller was fixed to a standard structure used in electron beam stabilisation, an additional output reference signal was introduced in closed loop. By aligning the reference signal with each mode, the MIMO identification problem was reduced to a SISO identification problem, allowing the sensitivity to be estimated mode-by-mode. We derived lower and upper bounds on the



(a) Magnitude of true complementary sensitivity,  $|\tilde{T}_i(j\omega)|$ .



(b) Magnitude of estimated complementary sensitivity,  $|\hat{T}_i(j\omega)|$ .



(c) Absolute error,  $|\tilde{T}_i(j\omega) - \hat{T}_i(j\omega)|$ .

Fig. 5: Complementary sensitivities and estimation error over modes and frequencies. For each mode, the normalised frequency ranges from 0 to  $\tilde{\omega}_i$ .

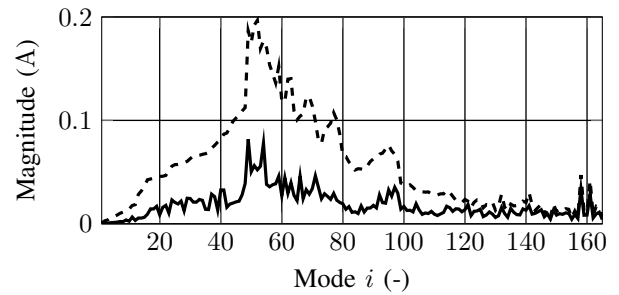


Fig. 6: Maximum input amplitudes in mode space (dashed) and original space (solid) for each iteration of Algorithm 1.

reference signal, which were used to tune the reference signal and bound the estimation error.

The derived bounds demonstrated the limitations imposed by the strong directionality of the system, requiring large reference amplitudes for identifying the sensitivity for higher-order modes, even when the dynamics of the reference signal are tuned to the modal closed-loop bandwidth. At the same time, higher-order modes require large input gains to follow the reference signal, conflicting with input magnitude constraints. While these limitations were evaluated using the parameters of the Diamond system, future research could focus on obtaining more general limits that are based on the condition number of the response matrix.

Although the simulations demonstrated that the estimation error remained within the expected bounds, the control inputs were well below the admissible maximum value. Firstly, this resulted from approximating the time-domain constraints in the frequency domain. Secondly, the frequency-domain constraints were enforced using a conservative upper bound, resulting in small input magnitudes for all modes. However, increasing input and reference magnitudes would benefit the signal-to-noise ratio on all modes. Future research could therefore focus developing less conservative bounds for the reference signal, e.g. using first principles or predictive control.

Throughout the paper, it was assumed that the plant model is accurate, allowing the MIMO system to be decoupled into sets of SISO systems. Although the Diamond synchrotron is regularly tuned to match its theoretical model, future research could investigate the effect of plant uncertainty, which impacts both the choice of the reference signal and the estimated sensitivity. These results could be further incorporated into a fault detection algorithm, which, in addition to evaluating the algorithm on the real-world system, is subject of future research.

## REFERENCES

- [1] S. Gayadeen and S. R. Duncan, "Discrete-time anti-windup compensation for synchrotron electron beam controllers with rate constrained actuators," *Automatica*, vol. 67, pp. 224–232, May 2016.
- [2] W. Heath, "Orthogonal functions for cross-directional control of web forming processes," *Automatica*, vol. 32, no. 2, pp. 183–198, February 1996.

- [3] J. G. Van Antwerp, A. P. Featherstone, R. D. Braatz, and B. A. Ogunnaike, "Cross-directional control of sheet and film processes," *Automatica*, vol. 43, no. 2, pp. 191–211, Feb. 2007.
- [4] S. Skogestad, M. Morari, and J. C. Doyle, "Robust control of ill-conditioned plants: high-purity distillation," *IEEE Trans. Automat. Contr.*, vol. 33, no. 12, pp. 1092–1105, December 1988.
- [5] S. Gayadeen and S. R. Duncan, "Design of an electron beam stabilisation controller for a synchrotron," *Contr. Eng. Pract.*, vol. 26, pp. 201–210, May 2014.
- [6] R. Bronès, A. Bence, J. Bisou, N. Hubert, D. Pédeau, and G. Pichon, "SOLEIL New Platform for Fast Orbit Feedback," *JACoW*, vol. IBIC2023, p. MO2C04, 2023.
- [7] D. G. Feingold and R. S. Varga, "Block diagonally dominant matrices and generalizations of the Gerschgorin circle theorem," *Pac. J. Math.*, vol. 12, no. 4, pp. 1241–1250, Apr. 1962.
- [8] G. H. Golub and C. F. Van Loan, *Matrix Computations*, 4th ed. Baltimore, MD: The Johns Hopkins Univ. Press, 2013.
- [9] I. Kempf, "Advanced control systems for fast orbit feedback of synchrotron electron beams," DPhil Thesis, Lady Margaret Hall, University of Oxford, Oxford, UK, 2023.
- [10] I. Kempf, M. Abbott, L. Bobb, G. Christian, S. Duncan, and G. Rehm, "Fast Orbit Feedback for Diamond-II," in *Proc. 12th Int. Beam Instrum. Conf. (IBIC'23)*, ser. International Beam Instrumentation Conference, no. 12. JACoW Publishing, Geneva, Switzerland, 12 2023, paper MO2I02, pp. 1–6.
- [11] I. Kempf, P. J. Goulart, S. R. Duncan, and M. Abbott, "Model predictive control for electron beam stabilization in a synchrotron," in *Proc. Eur. Contr. Conf. (ECC)*, London, UK, July 2022, pp. 814–819.
- [12] L. Ljung, *System Identification: Theory for the User*, 2nd ed. Upper Saddle River, NJ: Prentice-Hall, 1999.
- [13] P. Van den Hof, "Closed-loop issues in system identification," *Annu. Rev. Contr.*, vol. 22, pp. 173–186, 1998.